A FAST TEMPLATE PERIODOGRAM FOR DETECTING NON-SINUSOIDAL FIXED-SHAPE SIGNALS IN IRREGULARLY SAMPLED TIME SERIES
DRAFT VERSION 1

J. Hoffman[1], J. Vanderplas[2], J. Hartman[1], G. Bakos[1]

Draft version December 3, 2017

ABSTRACT

Astrophysical time series often contain periodic signals. The large and growing volume of time series data from photometric surveys demands computationally efficient methods for detecting and characterizing such signals. The most efficient algorithms available for this purpose are those that exploit the $\mathcal{O}(N \log N)$ scaling of the Fast Fourier Transform (FFT). However, these methods are not optimal for non-sinusoidal signal shapes. Template fits (or periodic matched filters) optimize sensitivity for *a priori* known signal shapes but at enormous computational cost. Current implementations of template periodograms scale as $\mathcal{O}(N_f N_{\mathrm{obs}})$, where N_f is the number of trial frequencies and N_{obs} is the number of lightcurve observations, and they do not gaurantee the best fit at each trial frequency. In this work, we present a non-linear extension of the Lomb-Scargle periodogram to obtain a template-fitting algorithm that is both accurate (optimal solutions are obtained except in rare cases) and computationally efficient (scaling as $\mathcal{O}(N_f \log N_f)$). The non-linear optimization of the template fit at each frequency is recast as a polynomial zero-finding problem, where the coefficients of the polynomial can be computed efficiently with the non-equispaced fast Fourier transform. We show that our method, which uses truncated Fourier series to approximate templates, is an order of magnitude faster than existing algorithms for small problems ($N \lesssim 10$ observations) and 2 orders of magnitude faster for long base-line time series with $\mathcal{O}(10^4)$ observations. An open-source implementation of the fast template periodogram is available at github.com/PrincetonUniversity/FastTemplatePeriodogram.

1. INTRODUCTION

Astronomical systems exhibit a wide range of time-dependent variability. By measuring and characterizing this variability, astronomers are able to infer a variety of important astrophysical properties about the underlying system.

Periodic signals in noisy astronomical timeseries can be detected with a number of techniques, including Gaussian process regression (Foreman-Mackey et al. 2017; Rasmussen & Williams 2005), least-squares spectral analysis (Lomb 1976; Scargle 1982; Barning 1963; Vaníček 1971), and information-theoretic methods (Graham et al. 2013a; Huijse et al. 2012; Cincotta et al. 1995). For an empirical comparison of some of these techniques applied to several astronomical survey datasets, see Graham et al. (2013b).

For stationary periodic signals, least-squares spectral analysis — also known as the Lomb-Scargle (LS) periodogram (Lomb 1976; Scargle 1982; Barning 1963; Vaníček 1971) — is perhaps the most sensitive and computationally efficient method of detection. The LS periodogram can be made to scale as $\mathcal{O}(N_f \log N_f)$, where N_f is the number of trial frequencies, by utilizing the non-equispaced fast Fourier transform (**?**, NFFT;) to evaluate frequency-dependent sums, or by 'extirpolating" irregularly spaced observations to a regular grid with Lagrange polynomials (Press & Rybicki 1989).

The LS periodogram fits the following model to a set

jah5@princeton.edu
[1] Department of Astrophysical Sciences, Princeton University, Princeton NJ 08540
[2] eScience Institute, University of Washington, Seattle, WA 98195

of observations:

$$\hat{y}_{\mathrm{LS}}(t|\theta,\omega) = \theta_0 \cos \omega t + \theta_1 \sin \omega t. \quad (1)$$

where $\omega = 2\pi/P$ is the (angular) frequency of the underlying signal, and θ_0 and θ_1 are the amplitudes of the signal. When the data y_i is composed of a sinusoidal component and a white noise component (i.e., when the measurement uncertainties are uncorrelated and Gaussian), the LS periodogram provides a maximum likelihood estimate for ω, θ_0, and θ_1.

The LS "power" $P_{LS}(\omega)$, analogous to the spectral power, has several definitions in the literature (Zechmeister & Kürster 2009), but we adopt the following definition throughout the paper:

$$P(\omega) = \frac{\chi_0^2 - \chi^2(\omega)}{\chi_0^2} \quad (2)$$

Where χ_0^2 is the weighted sum of squared residuals for a constant fit:

$$\chi_0^2 = \sum_i w_i (y_i - \bar{y})^2 \quad (3)$$

where $\bar{y} = \sum_i w_i y_i$ is the weighted mean of the observations, and $w_i \propto \sigma_i^{-2}$ are the normalized weights for each observations ($\sum_i w_i = 1$), and $\chi^2(\omega)$ is the weighted sum of squared residuals for the best-fit model $\hat{y}$ at a given trial frequency $\omega = 2\pi/P$ where P is the period:

$$\chi^2(\omega) = \min_\theta \sum_i w_i (y_i - \hat{y}(\omega t_i|\theta))^2 \quad (4)$$

1.1. Extending Lomb-Scargle

The LS periodogram has numerous extensions to account for, e.g., biased estimates of the mean brightness (Zechmeister & Kürster 2009), non-sinusoidal signals (Schwarzenberg-Czerny 1996; Palmer 2009), multi-band observations (VanderPlas & Ivezić 2015), and to mitigate overfitting of more flexible models via regularization (VanderPlas & Ivezić 2015). For a detailed review of the LS periodogram and its extensions, see ?.

The multi-harmonic LS periodogram (?Schwarzenberg-Czerny 1996; Palmer 2009, MHLS;), provides a more flexible model by adding harmonic components to the fit:

$$\hat{y}_{\mathrm{MHLS}}(t|\theta,\omega) = \theta_0 + \sum_{n=1}^{H} \theta_{2n}\cos n\omega t + \theta_{2n-1}\sin n\omega t. \quad (5)$$

Additional harmonics are important for modeling signals that, while stationary and periodic, are non-sinusoidal (e.g. RR Lyrae, eclipsing binaries, etc.).

However, the MHLS periodogram contains $2H+1$ free parameters while the original LS periodogram contains only 2 (3 if the mean brightness is considered a free parameter). Additional free parameters mean that MHLS is less sensitive to sinusoidal signals than the Lomb-Scargle periodogram. Tikhonov regularization (or L_2 regularization), which amounts to imposing a Gaussian prior on the harmonic amplitudes, provides may mitigate overfitting in the MHLS model (VanderPlas & Ivezić 2015), but L_2 regularization introduces bias into the amplitude estimates if strong regularization is used, or, if weak regularization is used, may not be sufficient to overcome the loss of sensitivity from increasing the number of free parameters in the model.

1.2. Template periodograms

If the signal shape is known a priori, then the number of free parameters needed for a model fit is the same as the original LS periodogram (with a floating mean component):

$$\hat{y}(t|\theta,\omega) = \theta_0 + \theta_1 \mathbf{M}(\omega t - \theta_2), \quad (6)$$

where $\mathbf{M} : [0, 2\pi) \rightarrow \mathcal{R}$ is a predefined periodic template. We refer to the periodogram corresponding to this model as the "template periodogram."

As is the case for the LS periodogram, the template periodogram is equivalent to a maximum-likelihood estimate of the model fit under the assumption that measurement uncertainties are gaussian and uncorrelated (i.e. white noise).

1.3. Computational scaling

The LS periodogram naively scales as $\mathcal{O}(N_f N_{\mathrm{obs}})$ where N_f is the number of trial frequencies and N_{obs} is the number of observations. However, the computation of the LS periodogram involves sums of trigonometric functions over the observations. When the observations are regularly sampled, the fast Fourier transform (FFT) (Cooley & Tukey 1965) can evaluate such sums efficiently and the LS periodogram scales as $\mathcal{O}(N_f \log N_f)$.

When the data is not regularly sampled, as is the case for most astronomical time series, the LS periodogram can be evaluated quickly in one of two popular ways. The first, by Press & Rybicki (1989) involves "extirpolating" irregularly sampled data onto a regularly sampled mesh, and then performing FFTs to evaluate the necessary sums. The second, as pointed out in Leroy (2012), is to use the non-equispaced FFT (NFFT) ? to evaluate the sums; this provides roughly an order of magnitude speedup over the Press & Rybicki (1989) algorithm, and both algorithms scale as $\mathcal{O}(N_f \log N_f)$ (Leroy 2012).

There is a growing population of alternative methods for detecting periodic signals in astrophysical data. Some of these methods can reliably outperform the LS periodogram, especially for non-sinusoidal signal shapes (see Graham et al. (2013b) for a recent empirical review of period finding algorithms). However, a key advantage the LS periodogram and its extensions is speed. Virtually all other "phase-folding" methods scale as $\mathcal{O}(N_{\mathrm{obs}} \times N_f)$, where N_{obs} is the number of observations and N_f is the number of trial frequencies, while the Lomb-Scargle periodogram scales as $\mathcal{O}(N_f \log N_f)$. The virtual independence of Lomb-Scargle on the number of observations (assuming $N_f \gtrsim N_{\mathrm{obs}}$) is especially attractive for lightcurves with $N_{\mathrm{obs}} \gg \log N_f \sim 50$.

Algorithmic efficiency will become increasingly important as the volume of data produced by astronomical observatories continues to grow larger. The HATNet survey (Bakos et al. 2004), for example, has already made $\mathcal{O}(10^4)$ observations of $\mathcal{O}(10^6 - 10^7)$ stars. The Gaia telescope (Gaia Collaboration et al. 2016) is set to produce $\mathcal{O}(10-100)$ observations of $\mathcal{O}(10^9)$ stars. The Large Synoptic Survey Telescope (LSST; LSST Science Collaboration et al. (2009)) will make $\mathcal{O}(10^2 - 10^3)$ observations of $\mathcal{O}(10^{10})$ stars during its operation starting in 2023.

This paper develops new extensions of least-squares spectral analysis for arbitrary signal shapes. For non-periodic signals this method is known as matched filter analysis, and can be extended to search for periodic signals by phase folding the data at different trial periods. We refer to the latter technique, the subject of this paper, as template fitting.

Recently, Sesar et al. (2016) found that template fitting significantly improved period and amplitude estimation for RR Lyrae in Pan-STARRS DR1 (Chambers et al. 2016). Since the signal shapes for RR Lyrae in various bandpasses are known a priori (see Sesar et al. (2010)), template fitting provides an optimal estimate of amplitude and period, given that the object is indeed an RR Lyrae star well modeled by at least one of the templates. Templates were especially crucial for Pan-STARRS data, since there are typically only 35 observations per source over 5 bands (Hernitschek et al. 2016), not enough to obtain accurate amplitudes empirically by phase-folding. By including domain knowledge (i.e. knowledge of what RR Lyrae lightcurves look like), template fitting allows for accurate inferences of amplitude even for undersampled lightcurves.

However, the improved accuracy comes at substantial computational cost: the template fitting procedure took 30 minutes per CPU per object, and Sesar et al. (2016) were forced to limit the number of fitted lightcurves ($\lesssim 1000$) in order to keep the computational costs to a reasonable level. Several cuts were made before the template fitting step to reduce the more than 1 million

Pan-STARRS DR1 objects to a small enough number, and each of these steps removes a small portion of RR Lyrae from the sample. Though this number was reported by Sesar et al. (2016) to be small ($\lesssim 2\%$), it may be possible to further improve the completeness of the final sample by applying template fits to a larger number of objects, which would require either more computational resources, more time, or, ideally, a more efficient template fitting procedure.

The paper is organized as follows. Section 2 poses the problem of template fitting in the language of least squares spectral analysis and derives the fast template periodogram. Section 3 describes a freely available implementation of the new template periodogram. Section 4 summarizes our results, addresses caveats, and discusses possible avenues for improving the efficiency of the current algorithm.

2. DERIVATIONS

We define a template $\mathbf{M}$

$$\mathbf{M} : [0, 1) \to \mathbb{R}, \tag{7}$$

as a mapping between the unit interval and the set of real numbers. We restrict our discussion to sufficiently smooth templates such that $\mathbf{M}$ can be adequately described by a truncated Fourier series

$$\hat{\mathbf{M}}(\omega t | H) = \sum_{n=1}^{H} [c_n \cos n\omega t + s_n \sin n\omega t] \tag{8}$$

for some $H > 0$. Formally, we require that for some relative error tolerance ϵ and for some maximum number of harmonics $H \lesssim 15$,

$$\forall t \in [0, 1) : \lim_{H \to \infty} \left| \mathbf{M}(t) - \hat{\mathbf{M}}(t | H) \right| = 0 \tag{9}$$

That the c_n and s_n values are *fixed* (i.e., they define the template) is the crucial difference between the template periodogram and the multi-harmonic Lomb-Scargle (Palmer 2009; ?), where c_n and s_n are *free parameters*.

We now construct a periodogram for this template. The periodogram assumes that an observed time series $S = \{(t_i, y_i, \sigma_i)\}_{i=1}^{N}$ can be modeled by a scaled, transposed template that repeats with period $2\pi/\omega$, i.e.

$$y_i \approx \hat{y}(\omega t_i | \theta, \mathbf{M}) = \theta_1 \mathbf{M}(\omega t_i - \theta_2) + \theta_3, \tag{10}$$

where $\theta \in \mathbb{R}^3$ is a set of model parameters.

The optimal parameters are the location of a local minimum of the (weighted) sum of squared residuals,

$$\chi^2(\theta, S) \equiv \sum_i w_i (y_i - \hat{y}(\omega t_i | \theta))^2, \tag{11}$$

and thus the following condition must hold for all three model parameters at the optimal solution $\theta = \theta_{\mathrm{opt}}$:

$$\left. \frac{\partial \chi^2}{\partial \theta_j} \right|_{\theta = \theta_{\mathrm{opt}}} = 0 \;\; \forall \theta_j \in \theta. \tag{12}$$

Note that we have implicitly assumed $\chi^2(\theta, S)$ is a C^1 differentiable function of θ, which requires that $\mathbf{M}$ is a C^1

differentiable function. Though this assumption could be violated if we considered a more complete set of templates, (e.g. a box function), our restriction to truncated Fourier series ensures C^1 differentiability.

Note that we also implicitly assume $\sigma_i > 0$ for all i and we will later assume that the variance of the observations y_i is non-zero. If there are no measurement errors, i.e. $\sigma_i = 0$ for all i, then uniform weights (setting $\sigma_i = 1$) should be used. If the variance of the observations y is zero, the periodogram is trivial and will be zero for all frequencies. We do not consider the case where $\sigma_i = 0$ for some observations i and $\sigma_j > 0$ for some observations j. In that case, the weighted least squares estimator is undefined.

We can derive a system of equations for θ_{opt} from the condition given in Equation 12. The explicit condition that must be met for each parameter θ_j is simplified below, using

$$\hat{y}_i = \hat{y}(\omega t_i | \theta) \tag{13}$$

and

$$\partial_j \hat{y}_i = \left. \frac{\partial \hat{y}(\omega t | \theta)}{\partial \theta_j} \right|_{t=t_i} \tag{14}$$

for brevity:

$$\begin{aligned} 0 &= \left. \frac{\partial \chi^2}{\partial \theta_j} \right|_{\theta = \theta_{\mathrm{opt}}} \\ &= -2 \sum_i w_i (y_i - \hat{y}_i)(\partial_j \hat{y})_i \end{aligned} \tag{15}$$

$$\sum_i w_i y_i (\partial_j \hat{y})_i = \sum_i w_i \hat{y}_i (\partial_j \hat{y})_i.$$

The above is a general result that extends to all least squares periodograms. To simplify derivations, we adopt the following notation:

$$\langle X \rangle \equiv \sum_i w_i X_i \tag{16}$$

$$\langle XY \rangle \equiv \sum_i w_i X_i Y_i \tag{17}$$

$$\mathrm{Cov}(X, Y) \equiv \langle XY \rangle - \langle X \rangle \langle Y \rangle \tag{18}$$

$$\mathrm{Var}(X) \equiv \mathrm{Cov}(X, X) \tag{19}$$

In addition, the transposed template $\mathbf{M}_{\theta_2} = \mathbf{M}(\omega t_i - \theta_2)$ can be expressed as

$$\mathbf{M}_{\theta_2}(\omega t) = \sum_n c_n \cos n\,(\omega t - \theta_2) \tag{20}$$

$$+ s_n \sin n\,(\omega t - \theta_2) \tag{21}$$

$$= \sum_n (c_n \cos n\theta_2 - s_n \sin n\theta_2) \cos n\omega t + \tag{22}$$

$$(s_n \cos n\theta_2 + c_n \sin n\theta_2) \sin n\omega t \tag{23}$$

$$= \sum_n \left(\alpha_n e^{in\theta_2} + \alpha_n^* e^{-in\theta_2}\right) \cos n\omega t + \tag{24}$$

$$\left(-i\left[\alpha_n e^{in\theta_2} - \alpha_n^* e^{-in\theta_2}\right]\right) \sin n\omega t \tag{25}$$

$$= \sum_n \left(\alpha_n \psi^n + \alpha_n^* \psi^{-n}\right) \cos n\omega t + \tag{26}$$

$$\left(-i\left[\alpha_n \psi^n - \alpha_n^* \psi^{-n}\right]\right) \sin n\omega t \tag{27}$$

$$= \sum_n A_n(\psi) \cos n\omega t + B_n(\psi) \sin n\omega t \tag{28}$$

where $\alpha_n = (c_n + is_n)/2$, and $\psi \equiv e^{i\theta_2}$ is a convenient change of variable.

We also define the following terms:

$$\widehat{YM} = \langle y\mathbf{M}_{\theta_2}\rangle \tag{29}$$

$$\widehat{MM} = \langle \mathbf{M}_{\theta_2}^2\rangle \tag{30}$$

$$\overline{M} = \langle \mathbf{M}_{\theta_2}\rangle \tag{31}$$

$$MM = \mathrm{Var}(\mathbf{M}_{\theta_2}) = \widehat{MM} - \overline{M}^2 \tag{32}$$

$$YM = \mathrm{Cov}(\mathbf{M}_{\theta_2}, y) = \widehat{YM} - \bar{y}\overline{M} \tag{33}$$

For a given phase shift θ_2, the optimal amplitude and offset are obtained from requiring the partial derivatives of the sum of squared residuals, χ^2, to be zero.

Namely, we obtain that

$$0 = \frac{\partial \chi^2}{\partial \theta_1} = 2\sum_i w_i(y_i - \hat{y}_i)\left(-\frac{\partial \hat{y}}{\partial \theta_1}\right)_i \tag{34}$$

$$= \sum_i w_i(y_i - \theta_1\mathbf{M}_{\theta_2} - \theta_3)\mathbf{M}_{\theta_2} \tag{35}$$

$$= \widehat{YM} - \theta_1\widehat{MM} - \theta_3\overline{M} \tag{36}$$

and

$$0 = \frac{\partial \chi^2}{\partial \theta_3} = 2\sum_i w_i(y_i - \hat{y}_i)\left(-\frac{\partial \hat{y}}{\partial \theta_3}\right)_i \tag{37}$$

$$= \sum_i w_i(y_i - \theta_1\mathbf{M}_{\theta_2} - \theta_3) \tag{38}$$

$$= \bar{y} - \theta_1\overline{M} - \theta_3 \tag{39}$$

This system of equations can then be rewritten as

$$\begin{pmatrix} \widehat{MM} & \overline{M} \\ \overline{M} & 1 \end{pmatrix}\begin{pmatrix} \theta_1 \\ \theta_3 \end{pmatrix} = \begin{pmatrix} \widehat{YM} \\ \bar{y} \end{pmatrix} \tag{40}$$

which reduces to

$$\begin{pmatrix} \theta_1 \\ \theta_3 \end{pmatrix} = \frac{1}{\widehat{MM} - \overline{M}^2}\begin{pmatrix} 1 & -\overline{M} \\ -\overline{M} & \widehat{MM} \end{pmatrix}\begin{pmatrix} \widehat{YM} \\ \bar{y} \end{pmatrix} \tag{41}$$

$$= \frac{1}{\widehat{MM} - \overline{M}^2}\begin{pmatrix} \widehat{YM} - \bar{y}\overline{M} \\ \widehat{MM}\bar{y} - \widehat{YM}\overline{M} \end{pmatrix} \tag{42}$$

Letting $MM = \widehat{MM} - \overline{M}^2$ and $YM = \widehat{YM} - \bar{y}\overline{M}$, we have

$$\begin{pmatrix} \theta_1 \\ \theta_3 \end{pmatrix} = \begin{pmatrix} YM/MM \\ \bar{y} - \overline{M}(YM/MM) \end{pmatrix} \tag{43}$$

This means we can rewrite the model $\hat{y} = \theta_1\mathbf{M}_{\theta_2} + \theta_3$ as

$$\hat{y}_i = \bar{y} + \left(\frac{YM}{MM}\right)(M_i - \overline{M}) \tag{44}$$

To obtain an expression for the periodogram, $P = 1 - \chi^2/\chi_0^2$, we first compute χ^2

$$\chi^2 = \sum_i w_i(y_i - \hat{y}_i)^2 \tag{45}$$

$$= \sum_i w_i(y_i^2 - 2y_i\hat{y}_i + \hat{y}_i^2) \tag{46}$$

$$= YY - 2\frac{(YM)^2}{MM} + \frac{(YM)^2}{MM} \tag{47}$$

$$= YY - \frac{(YM)^2}{MM} \tag{48}$$

Since, $\chi_0^2 = YY$, we have

$$P(\omega) = \frac{(YM)^2}{YY \cdot MM} \tag{49}$$

We wish to maximize $P(\omega)$ with respect to the phase shift parameter θ_2,

$$\partial_{\theta_2}P = 0 = \frac{YM}{YY \cdot MM}\left(2\partial_{\theta_2}(YM) - \frac{YM}{MM}\partial_{\theta_2}(MM)\right) \tag{50}$$

$$= 2MM\partial_{\theta_2}(YM) - YM\partial_{\theta_2}(MM). \tag{51}$$

The final expression is the non-linear condition that must be satisfied by the optimal phase shift parameter θ_2. However, satisfying Equation 50 is not *sufficient* to guarantee that θ_2 is optimal. The value of the periodogram at each θ_2 satisfying Equation 50 must be computed, and the globally optimal solution chosen from this set.

We seek a more explicit form for Equation 50. We derive expressions for MM and YM, defining

$$CC_{nm} \equiv \mathrm{Cov}(\cos n\omega t, \cos m\omega t) \tag{52}$$

$$CS_{nm} \equiv \mathrm{Cov}(\cos n\omega t, \sin m\omega t) \tag{53}$$

$$SS_{nm} \equiv \mathrm{Cov}(\sin n\omega t, \sin m\omega t) \tag{54}$$

$$YC_n \equiv \langle(y - \bar{y})\cos n\omega t\rangle \tag{55}$$

$$YS_n \equiv \langle(y - \bar{y})\sin n\omega t\rangle. \tag{56}$$

,

all of which can be evaluated efficiently using non-equispaced fast Fourier transforms (NFFT).

The autocovariance of the template values MM, is given by

$$MM \equiv \sum_i w_i M_i^2 - \left(\sum_i w_i M_i \right)^2 \tag{57}$$

$$= \sum_i w_i \left(\sum_n A_n \cos \omega n t_i + B_n \sin \omega n t_i \right)^2 \tag{58}$$

$$- \left(\sum_n A_n C_n + B_n S_n \right)^2 \tag{59}$$

$$= \sum_{n,m} A_n A_m CC_{nm}$$
$$+ (A_n B_m CS_{nm} + B_n A_m (CS^T)_{nm})$$
$$+ B_n B_m SS_{nm} \tag{60}$$

$$= \sum_{n,m} A_n A_m CC_{nm} + 2 A_n B_m CS_{nm}$$
$$+ B_n B_m SS_{nm}, \tag{61}$$

where we have used the fact that
as well as their products

$$A_n A_m = \left(\alpha_n \psi^n + \alpha_n^* \psi^{-n} \right) \left(\alpha_m \psi^m + \alpha_m^* \psi^{-m} \right)$$
$$= \alpha_n \alpha_m \psi^{n+m} + \alpha_n^* \alpha_m \psi^{m-n}$$
$$+ \alpha_n \alpha_m^* \psi^{n-m} + \alpha_n^* \alpha_m^* \psi^{-n-m)} \tag{62}$$

$$A_n B_m = -i \left(\alpha_n \psi^n + \alpha_n^* \psi^{-n} \right) \left(\alpha_m \psi^m - \alpha_m^* \psi^{-m} \right)$$
$$= -i \left\{ \alpha_n \alpha_m \psi^{n+m} + \alpha_n^* \alpha_m \psi^{m-n} \right.$$
$$\left. - \alpha_n \alpha_m^* \psi^{n-m} - \alpha_n^* \alpha_m^* \psi^{-n-m)} \right\} \tag{63}$$

$$B_n B_m = - \left(\alpha_n \psi^n - \alpha_n^* \psi^{-n} \right) \left(\alpha_m \psi^m - \alpha_m^* \psi^{-m} \right)$$
$$= - \left\{ \alpha_n \alpha_m \psi^{n+m} - \alpha_n^* \alpha_m \psi^{m-n} \right.$$
$$\left. - \alpha_n \alpha_m^* \psi^{n-m} + \alpha_n^* \alpha_m^* \psi^{-n-m} \right\} \tag{64}$$

Now we have that

$$MM_{nm} = A_n A_m CC_{nm} + 2 A_n B_m CS_{nm} + B_n B_m SS_{nm}$$
$$= \alpha_n \alpha_m \widetilde{CC}_{nm} \psi^{n+m} + 2 \alpha_n \alpha_m^* \widetilde{CS}_{nm} \psi^{n-m}$$
$$+ \alpha_n^* \alpha_m^* \widetilde{SS}_{nm} \psi^{-(n+m)} \tag{65}$$

where

$$\widetilde{CC}_{nm} = (CC_{nm} - SS_{nm}) - i \left(CS + CS^T \right)_{nm} \tag{66}$$

$$\widetilde{CS}_{nm} = (CC_{nm} + SS_{nm}) + i \left(CS - CS^T \right)_{nm} \tag{67}$$

$$\widetilde{SS}_{nm} = (CC_{nm} - SS_{nm}) + i \left(CS + CS^T \right)_{nm} \tag{68}$$

and for YM:

$$YM_k = A_k YC_k + B_k YS_k$$
$$= \alpha_k YC_k \psi^k + \alpha_k^* YC_k \psi^{-k}$$
$$- i \left(\alpha_k YS_k \psi^k - \alpha_k^* YS_k \psi^{-k} \right)$$
$$= (YC_k - iYS_k) \alpha_k \psi^k + (YC_k + iYS_k) \alpha_k^* \psi^{-k}$$
$$= \alpha_k \widetilde{YC}_k \psi^k + \alpha_k^* \widetilde{YC}_k^* \psi^{-k}. \tag{69}$$

We also define $YM' = \psi^H YM$ and $MM' = \psi^{2H} MM$, both of which are polynomials. Their derivatives are

$$\partial YM' = H \psi^{H-1} YM + \psi^H \partial YM \tag{70}$$

$$\partial MM' = 2H \psi^{2H-1} MM + \psi^{2H} \partial MM. \tag{71}$$

A new polynomial condition can then be expressed in terms of MM', YM' and their derivatives.

$$0 = 2MM \partial(YM) - YM \partial(MM) \tag{72}$$

$$= \psi^{3H+1} \left(2MM \partial(YM) - YM \partial(MM) \right) \tag{73}$$

$$= 2\psi^{2H} MM \left(\psi^{H+1} \partial(YM) \right)$$
$$- \psi^H YM \left(\psi^{2H+1} \partial(MM) \right) \tag{74}$$

$$= 2MM' \left(\psi \partial(YM') - H(YM') \right)$$
$$- YM' \left(\psi \partial(MM') - 2H(MM') \right) \tag{75}$$

$$= \psi \left(2MM' \partial(YM') - YM' \partial(MM') \right)$$
$$- 2H \left(MM' YM' - YM' MM' \right) \tag{76}$$

$$= 2MM' \partial(YM') - YM' \partial(MM') \tag{77}$$

The last step assumes that $\psi \neq 0$, which is a valid assumption since $\psi = e^{i\theta_2}$ lies on the unit circle for all real θ_2.

We solve for the zeros of the polynomial condition defined by Equation 72 using the `numpy.polynomial.polyroots` function, which solves for the eigenvalues of the polynomial companion matrix. Of resulting roots r_i produced by the `numpy.polynomial.polyroots`, only those that are close to the unit circle are kept (i.e. $|r_i - 1| < \delta$, with $\delta = 0.1$).

Solving for the zeros of a polynomial given a set of coefficients is unstable in certain cases, since the coefficients are represented as floating point numbers with finite precision. Thus, we scale the roots by their modulus to ensure they lie on the unit circle. Alternatively, we could use iterative schemes such as Newton's method to improve the estimate of the roots more robustly, however this requires more computational power and the accuracy of the roots was not a problem for any of the test cases we performed.

2.1. Negative amplitude solutions

The model $\hat{y} = \theta_1 \mathbf{M}_{\theta_2} + \theta_0$ allows for $\theta_1 < 0$ solutions. In the original formulation of Lomb-Scargle and in linear extensions involving multiple harmonics, negative amplitudes translate to phase differences, since $-\cos x = \cos(x - \pi)$ and $-\sin x = \sin(x - \pi)$.

However, for non-sinusoidal templates, $\mathbf{M}$, negative amplitudes do not generally correspond to a phase difference. For example, a detached eclipsing binary template $\mathbf{M}_{\text{EB}}(x)$ cannot be expressed in terms of a phase-shifted negative eclipsing binary template; i.e. $\mathbf{M}_{\text{EB}} \neq -\mathbf{M}_{\text{EB}}(x - \phi)$ for any $\phi \in [0, 2\pi)$.

Negative amplitude solutions found by the fast template periodogram are usually undesirable, as they may produce false positives for lightcurves that resemble flipped versions of the desired template, and allowing for $\theta_1 < 0$ solutions increases the number of effective free parameters of the model, which lowers the signal to noise, especially for weak signals.

One possible remedy for this problem is to set $P_{\text{FTP}}(\omega) = 0$ if the optimal solution for θ_1 is negative, but this complicates the interpretation of P_{FTP}. Another possible remedy is, for frequencies that have a $\theta_1 < 0$ solution, to search for the optimal parameters while enforcing that $\theta_1 > 0$, e.g. via non-linear optimization, but this likely will eliminate the computational advantage of FTP over existing methods.

Thus, we allow for negative amplitude solutions in the model fit and caution the user to check that the best fit θ_1 is positive. Negative amplitude solutions may only be a problem for weak signals, or signals that, when flipped, are similar to other astrophysical signals.

2.2. Extending to multi-band observations
2.2.1. Multi-phase model

As shown in VanderPlas & Ivezić (2015), the multi-phase periodogram (their $(N_{\text{base}}, N_{\text{band}}) = (0, 1)$ periodogram), for any model can be expressed as a linear combination of single-band periodograms:

$$P^{(0,1)}(\omega) = \frac{\sum_{k=1}^{K} \chi_{0,k}^2 P_k(\omega)}{\sum_{k=1}^{K} \chi_{0,k}^2} \qquad (78)$$

where K denotes the number of bands, $\chi_{0,k}^2$ is the weighted sum of squared residuals between the data in the k-th band and its weighted mean $\langle y \rangle$, and $P_k(\omega)$ is the periodogram value of the k-th band at the trial frequency ω.

With Equation 78, the template periodogram is readily applicable to multi-band time series, which is crucial for experiments like LSST, SDSS, Pan-STARRS, and other current and future photometric surveys.

2.2.2. Shared-phase model

Extending the template periodogram to multi-band observations while fixing the relative phases of the templates requires additional derivation. A shared-phase model has $2K + 1$ free parameters, with an offset and amplitude for each filter and a shared phase term.

The χ^2 corresponding to the shared-phase multiband model is

$$\chi^2 = \sum_{i}^{K} \sum_{j}^{N_i} w_j^{(i)} (y_j^{(i)} - \hat{y}_j^{(i)})^2, \qquad (79)$$

where $\hat{y}_j^{(i)} = \theta_1^{(i)} \mathbf{M}_{\theta_2}^{(i)} + \theta_3^{(i)}$ represents the model corresponding to a given filter i. The system of equations derived by setting $\partial_\theta \chi^2 = 0$ for each parameter θ reduces to the familiar expressions for the amplitude and offset:

$$\theta_1^{(i)} = \frac{\left\langle (y_j^{(i)} - \bar{y}^{(i)}) \mathbf{M}_{\theta_2}^{(i)} \right\rangle}{\text{Var}(\mathbf{M}_{\theta_2}^{(i)})} \qquad (80)$$

$$\theta_3^{(i)} = \bar{y}^{(i)} - \theta_1^{(i)} \text{Var}(\mathbf{M}_{\theta_2}^{(i)}), \qquad (81)$$

as well as a non-linear relation that must be satisfied for the shared-phase parameter:

$$\sum_{i}^{M} \left\langle (y_j^{(i)} - \bar{y}^{(i)}) \mathbf{M}_{\theta_2}^{(i)} \right\rangle \left(\prod_{k \neq i} \left(\text{Var}\left(\mathbf{M}_{\theta_2}^{(k)} \right) \right)^2 \right) \qquad (82)$$

$$\times \left(\left\langle (y_j^{(i)} - \bar{y}^{(i)}) \partial \mathbf{M}_{\theta_2}^{(i)} \right\rangle \text{Var}\left(\mathbf{M}_{\theta_2}^{(i)} \right) - \left\langle (y_j^{(i)} - \bar{y}^{(i)}) \mathbf{M}_{\theta_2}^{(i)} \right\rangle \text{Cov}\left(\mathbf{M}_{\theta_2}^{(i)}, \partial \mathbf{M}_{\theta_2}^{(i)} \right) \right) = 0. \qquad (83)$$

2.2.3. Other multi-band extensions

Other multi-band template periodograms are derivable; for instance, Sesar et al. (2016) used what amounted to a shared phase, amplitude, and offset model. Their model can be translated to

$$\hat{y}_j^{(i)} = \theta_1 \left(\underbrace{\alpha^{(i)} \mathbf{M}_{\theta_2}^{(i)} + \beta^{(i)}}_{\widetilde{M}_{\theta_2}^{(i)}} \right) + \theta_3 \qquad (84)$$

where the $\alpha^{(i)}$ and $\beta^{(i)}$ parameters are fixed. This

model has only 3 free parameters, which allowed Sesar et al. (2016) to achieve high signal-to-noise despite having less than 10 epochs in each band.

In this case, the requirement that $\partial_{\theta_1} \chi^2 = 0$ gives

$$0 = \sum_{i}^{K} \left\langle y_j^{(i)} \widetilde{M}_{\theta_2}^{(i)} \right\rangle - \theta_1 \sum_{i}^{K} \left\langle \left(\widetilde{M}_{\theta_2}^{(i)} \right)^2 \right\rangle \qquad (85)$$

$$- \theta_3 \sum_{i}^{K} \left\langle \widetilde{M}_{\theta_2}^{(i)} \right\rangle. \qquad (86)$$

Requiring $\partial_{\theta_3}\chi^2 = 0$ gives another relation between the offset and amplitude parameters

$$0 = \sum_i^K \bar{y}^{(i)} - \theta_1 \sum_i^K \left\langle \widetilde{M}_{\theta_2}^{(i)} \right\rangle - K\theta_3 \qquad (87)$$

$$\implies \theta_3 = \overline{\bar{y}^{(i)}} - \theta_1 \overline{\left\langle \widetilde{M}_{\theta_2}^{(i)} \right\rangle}. \qquad (88)$$

which implies that

$$0 = \sum_i^K \left\langle y_j^{(i)} \widetilde{M}_{\theta_2}^{(i)} \right\rangle - \theta_1 \sum_i^K \left\langle \left(\widetilde{M}_{\theta_2}^{(i)} \right)^2 \right\rangle \qquad (89)$$

$$- K\overline{\bar{y}^{(i)}} \overline{\left\langle \widetilde{M}_{\theta_2}^{(i)} \right\rangle} + K\theta_1 \overline{\left\langle \widetilde{M}_{\theta_2}^{(i)} \right\rangle}^2 \qquad (90)$$

$$= \overline{\left\langle (y_j^{(i)} - \overline{\bar{y}^{(i)}}) \widetilde{M}_{\theta_2}^{(i)} \right\rangle} - \theta_1 \left(\overline{\left\langle \left(\widetilde{M}_{\theta_2}^{(i)} \right)^2 \right\rangle} \right) \qquad (91)$$

$$- \overline{\left\langle \widetilde{M}_{\theta_2}^{(i)} \right\rangle}^2 \right) \qquad (92)$$

$$\theta_1 = \frac{\overline{\left\langle (y_j^{(i)} - \overline{\bar{y}^{(i)}}) \widetilde{M}_{\theta_2}^{(i)} \right\rangle}}{\overline{\left\langle \left(\widetilde{M}_{\theta_2}^{(i)} \right)^2 \right\rangle} - \overline{\left\langle \widetilde{M}_{\theta_2}^{(i)} \right\rangle}^2} \qquad (93)$$

Where here, $\bar{\cdot}$ denotes a quantity averaged over all bandpasses. Combining these relations with the requirement that $\partial_{\theta_2}\chi^2 = 0$, i.e.

$$0 = \theta_1 \sum_i^M \left\langle y_j^{(i)} \partial \widetilde{M}_{\theta_2}^{(i)} \right\rangle - \theta_1 \left\langle \widetilde{M}_{\theta_2}^{(i)} \partial \widetilde{M}_{\theta_2}^{(i)} \right\rangle \qquad (94)$$

$$- \theta_3 \left\langle \partial \widetilde{M}_{\theta_2}^{(i)} \right\rangle, \qquad (95)$$

produces the condition that must be satisfied by the optimal phase parameter θ_2,

$$\overline{\left\langle (y_j^{(i)} - \overline{\bar{y}^{(i)}}) \partial \widetilde{M}_{\theta_2}^{(i)} \right\rangle} \left(\overline{\left\langle \left(\widetilde{M}_{\theta_2}^{(i)} \right)^2 \right\rangle} - \overline{\left\langle \widetilde{M}_{\theta_2}^{(i)} \right\rangle}^2 \right) - \overline{\left\langle (y_j^{(i)} - \overline{\bar{y}^{(i)}}) \widetilde{M}_{\theta_2}^{(i)} \right\rangle} \left(\overline{\left\langle \widetilde{M}_{\theta_2}^{(i)} \partial \widetilde{M}_{\theta_2}^{(i)} \right\rangle} - \overline{\left\langle \widetilde{M}_{\theta_2}^{(i)} \right\rangle \left\langle \partial \widetilde{M}_{\theta_2}^{(i)} \right\rangle} \right). \qquad (96)$$

2.3. Computational requirements

For a given number of harmonics H, the task of deriving the polynomial given in 72 requires $\mathcal{O}(H^2)$ computations, and finding roots requires $\mathcal{O}(H^3)$ computations. The degree of the final polynomial is $6H - 1$.

When considering N_f trial frequencies, the polynomial computation and root-finding step scales as $\mathcal{O}(H^3 N_f)$. The computation of the sums (Equations $52 - 56$) scales as $\mathcal{O}(H N_f \log H N_f)$. Therefore, the entire template periodogram scales as

$$\mathcal{O}(H N_f \log H N_f + H^3 N_f). \qquad (97)$$

For a fixed number of harmonics H, the template periodogram scales as $\mathcal{O}(N_f \log N_f)$. However, for a constant number of trial frequencies N_f, the template algorithm scales as $\mathcal{O}(H^3)$, and computational resources alone limit H to reasonably small numbers $H \lesssim 15$ (see Figure 1).

2.3.1. Computational considerations of multi-band extensions

Multi-band extensions generally require more computational time than the single band case. For the shared-phase multi-band periodogram, the scaling becomes $\mathcal{O}KHN_f \log HN_f + K^3 H^3 N_f$. The final expression given in Equation 82 produces a root-finding polynomial that is of order $2H(5K - 1)$ for $K > 1$, compared

with the order $\sim 6H$ polynomial obtained for the $K = 1$ case.

For the shared phase, amplitude, and offset case, however, the polynomial order remains the same as for the single band case, though the time needed to compute the polynomial coefficients increases by a factor of K.

3. IMPLEMENTATION

An open-source implementation of the template periodogram in Python is available.[3] Polynomial algebra is performed using the `numpy.polynomial` module (Jones et al. 2001–). The `nfft` Python module, [4] which provides a Python implementation of the non-equispaced fast Fourier transform (?), is used to compute the necessary sums for a particular time series.

No explicit parallelism is used anywhere in the current implementation, however certain linear algebra operations in `Scipy` use OpenMP via calls to BLAS libraries that have OpenMP enabled.

All timing tests were run on a quad-core 2.6 GHz Intel Core i7 MacBook Pro laptop (mid-2012 model) with 8GB of 1600 MHz DDR3 memory. The `Scipy` stack (version 0.18.1) was compiled with multi-threaded MKL libraries.
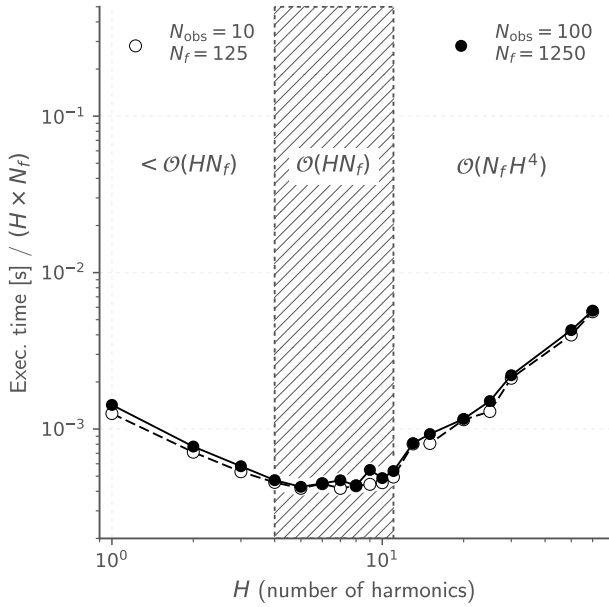
---

[3] https://github.com/PrincetonUniversity/FastTemplatePeriodogram
[4] https://github.com/jakevdp/nfft

FIG. 1.— Computation time of FTP scaled by NH for different numbers of harmonics. For $H \lesssim 3$, FTP scales sublinearly in H (possibly due to a constant overhead per trial frequency, independent of H). When $3 \lesssim H \lesssim 11$, FTP scales approximately linearly in H, and when $H \gtrsim 11$ FTP approaches the $\mathcal{O}(H^3)$ scaling limit.

3.1. Comparison with non-linear optimization

Within the Python implementation of the FTP, we have provided access to slower methods that employ non-linear optimizationto compare the accuracy and speed of the template periodogram described in this paper.

Periodograms computed in Figures 2, 3, and 4 used simulated data. The simulated data has uniformly random observation times, with gaussian-random, homoskedastic, uncorrelated uncertainties. An eclipsing binary template, generated by fitting a well-sampled, high signal-to-noise eclipsing binary in the HATNet dataset (BD+56 603) with a 10-harmonic truncated Fourier series.

3.1.1. Accuracy

For weak signals or signals folded at the incorrect trial period, there may be a large number of local χ^2 minima in the parameter space, and thus non-linear optimization algorithms may have trouble finding the global minimum. The FTP, on the other hand, solves for the optimal parameters directly, and thus is able to recover optimal solutions even when the signal is weak or not present.

Figure 3 illustrates the accuracy improvement with FTP. Many solutions found via non-linear optimization are significantly suboptimal compared to the solutions found by the FTP.

Figure 4 compares FTP results obtained using the full template ($H = 10$) with those obtained using smaller numbers of harmonics. The left-most plot compares the $H = 1$ case (weighted Lomb-Scargle), which, as also demonstrated in Figure 2, illustrates the advantage of the template periodogram for known, non-sinusoidal signal shapes.

3.1.2. Computation time

FTP scales asymptotically as $\mathcal{O}(N_f H \log N_f H)$ with respect to the number of trial frequencies, N_f and as $\mathcal{O}(N_f H^3 t)$ with respect to the number of harmonics in which the template is expanded, H. However, for reasonable cases ($N_f \lesssim 10^{120}$ when $H = 5$) the computation time is dominated by computing polynomial coefficients and root finding, both of which scale linearly in N_f.

The number of trial frequencies needed for finding astrophysical signals in a typical photometric time series is

$$N_f = 1.75 \times 10^6 \left(\frac{\text{baseline}}{10 \text{ yrs}}\right) \left(\frac{\alpha}{5}\right) \left(\frac{15 \text{ mins}}{P_{\min}}\right) \quad (98)$$

where α represents the "oversampling factor," $\Delta f_{\text{peak}}/\Delta f$, where $\Delta f_{\text{peak}} \sim 1/\text{baseline}$ is the typical width of a peak in the periodogram and Δf is the frequency spacing of the periodogram.

Extrapolating from the timing of a test case (500 observations, 5 harmonics, 15,000 trial frequencies), the summations account for approximately 5% of the computation time when $N_f \sim 10^6$. If polynomial computations and root-finding can be improved to the point where they no longer dominate the computation time, this would provide an order of magnitude speedup over the current implementation.

Figure 5 compares the timing of the FTP with that of previous methods that employ non-linear optimization. For the case when $N_f \propto N_{\text{obs}}$, FTP achieves a factor of 3 speedup for even the smallest test case (15 datapoints), while for larger cases ($N \sim 10^4$) FTP offers 2-3 orders of magnitude speed improvement. For the constant baseline case, FTP is a factor of ~ 2 faster for the smallest test case and a factor of ~ 20 faster for $N_{\text{obs}} \sim 10^4$. Future improvements to the FTP implementation could further improve speedups by 1-2 orders of magnitude over non-linear optimization.

4. DISCUSSION

Template fitting is a powerful technique for accurately recovering the period and amplitude of objects with a priori known lightcurve shapes. It has been used in the literature by, e.g. Sesar et al. (2016, 2010), to analyze RR Lyrae in the SDSS and PS1 datasets, where it has been shown to produce purer samples of RR Lyrae at a given completeness. The computational cost of current template fitting algorithms, however, limits their application to larger datasets or with a larger number of templates.

We have presented a novel template fitting algorithm that extends the Lomb-Scargle periodogram (Lomb 1976; Scargle 1982; Barning 1963; Vaníček 1971) to handle non-sinusoidal signals that can be expressed in terms of a truncated Fourier series with a reasonably small number of harmonics ($H \lesssim 10$).

The fast template periodogram (FTP) asymptotically scales as $\mathcal{O}(N_f H \log N_f H + N_f H^4)$, while previous template fitting algorithms such as the one used in the gatspy library (VanderPlas 2016), scale as $\mathcal{O}(N_f N_{\text{obs}})$. However, the FTP effectively scales as $\mathcal{O}(N_f H^4)$, since the time needed to compute polynomial coefficients and perform zero-finding dominates the computational time
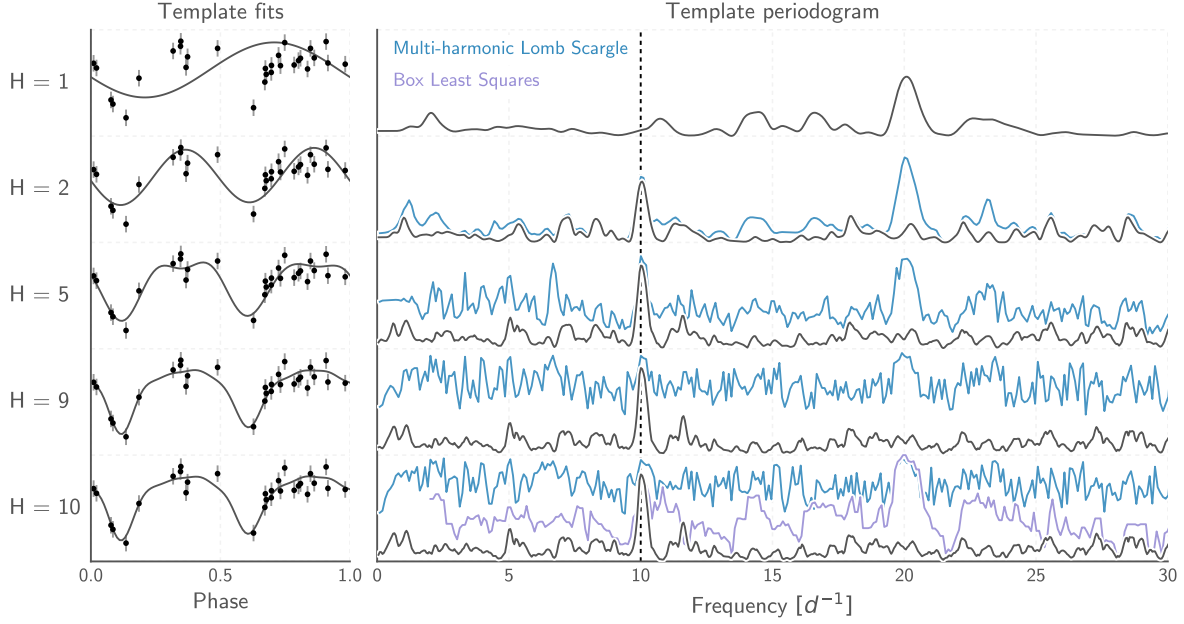
FIG. 2.— Template periodograms performed on a simulated eclipsing binary lightcurve (shown phase-folded in the left-hand plots). The top-most plot uses only one harmonic, equivalent to a Lomb-Scargle periodogram. Subsequent plots use an increasing number of harmonics, which produces a narrower and higher peak height around the correct frequency. For comparison, the multi-harmonic extension to Lomb-Scargle is plotted in blue, using the same number of harmonics as the FTP. The Box Least-Squares (Kovács et al. 2002) periodogram is shown in the final plot.
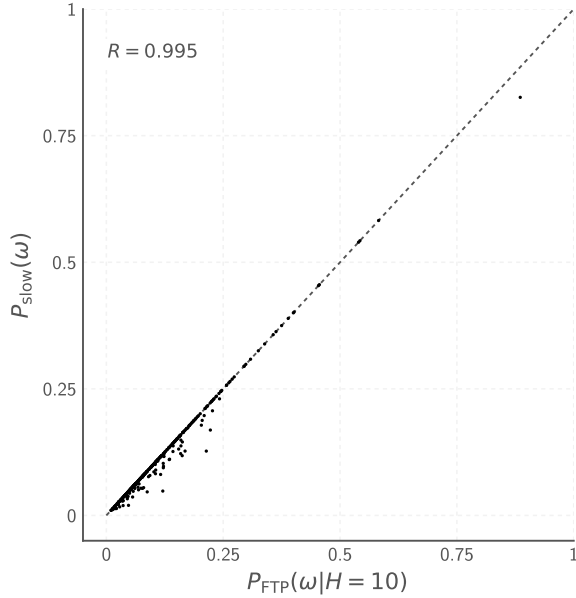
FIG. 3.— Comparing accuracy between previous methods that rely on non-linear optimization at each trial frequency with the fast template periodogram described in this paper. Both methods are applied to the same simulated data as shown in Figure 2. The FTP consistently finds more optimal template fits than those found with non-linear optimization, which do not gaurantee convergence to a globally optimal solution. The FTP solves for the optimal fit parameters directly, and therefore is able to achieve greater accuracy than template fits done via non-linear optimization.

for all practical cases ($N_f \lesssim 10^{120}$). The H^4 scaling effectively restricts templates to those that are sufficiently smooth to be explained by a small number of Fourier terms.

FTP also improves the accuracy of previous template fitting algorithms, which rely on non-linear optimization at each trial frequency to minimize the χ^2 of the template fit. The FTP routinely finds superior fits over non-linear optimization methods.

An open-source Python implementation of the FTP is available at GitHub.[5] The current implementation could likely be improved by:

1. Improving the speed of the polynomial coefficient calculations and the zero-finding steps. This could potentially yield a speedup of $\sim 1 - 2$ orders of magnitude over the current implementation.

2. Exploiting the embarassingly parallel nature of the FTP using GPU's.

For a constant baseline, the current implementation improves existing methods by factors of a $\sim$few for lightcurves with $\mathcal{O}(100)$ observations, and by an order of magnitude or more for objects with more than 1,000 observations. These improvements, taken at face value, are not enough to make template fitting feasible on LSST-sized datasets. However, optimizing the polynomial computations could yield a factor of $\sim 25 - 100$ speedup over the current implementation, which would make the FTP 1-3 orders of magnitude faster than alternative techniques.

[5] https://github.com/PrincetonUniversity/FastTemplatePeriodogram
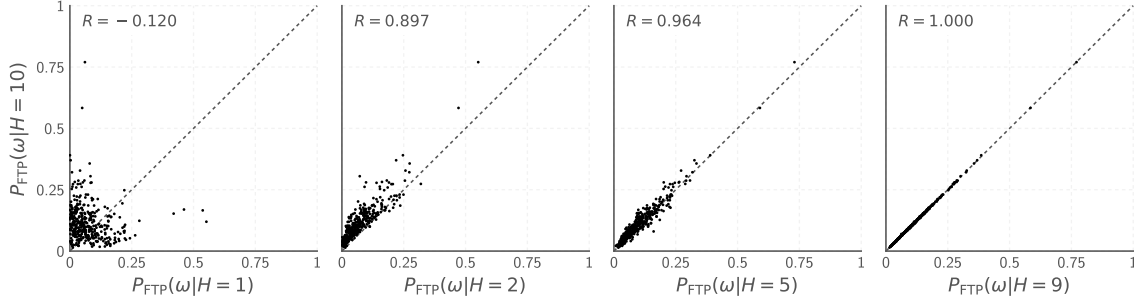
FIG. 4.— Comparing the template periodogram calculated with $H = 10$ harmonics to the template periodogram using a smaller number of harmonics $H < 10$. The template and data used to perform the periodogram calculations are the same as those shown in Figure 2.
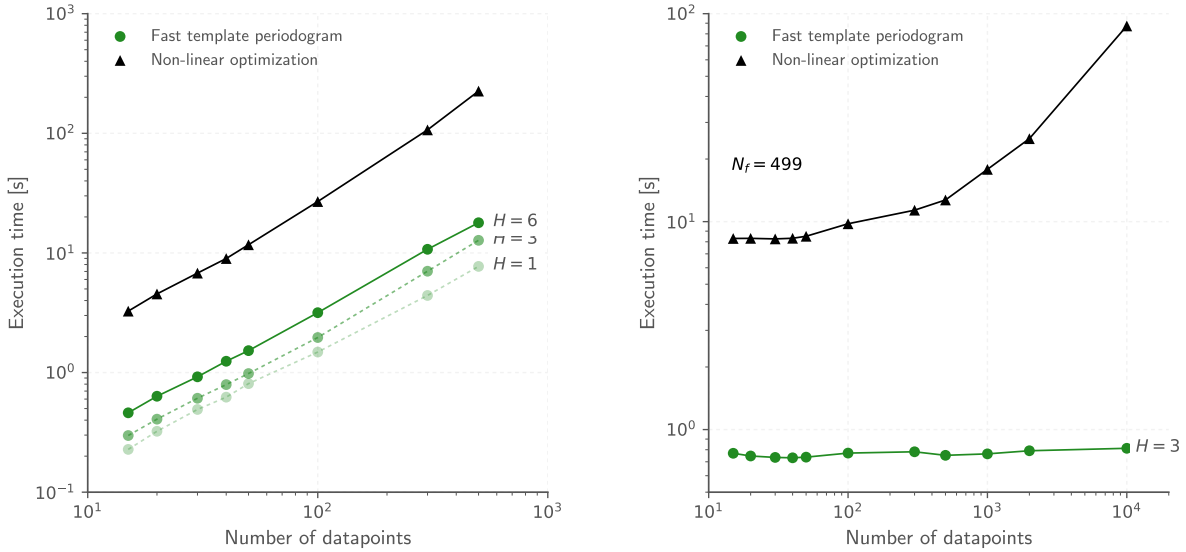

FIG. 5.— Computation time of FTP compared with alternative techniques that use non-linear optimization at each trial frequency. *Left*: timing for the case when $N_f = 12N_{\rm obs}$, i.e. the cadence of the observations is constant. *Right*: timing for the case when N_f is fixed, i.e. the baseline of the observations are constant. Non-linear optimization techniques scale as $\mathcal{O}(N_f N_{\rm obs})$ while the FTP scales as $\mathcal{O}(HN_f \log HN_f + N_f H^3)$, where H is the number of harmonics needed to approximate the template.

REFERENCES

Bakos, G., Noyes, R. W., Kovács, G., et al. 2004, PASP, 116, 266 1.3
Barning, F. J. M. 1963, Bull. Astron. Inst. Netherlands, 17, 22 1, 4
Chambers, K. C., Magnier, E. A., Metcalfe, N., et al. 2016, ArXiv e-prints, arXiv:1612.05560 1.3
Cincotta, P. M., Mendez, M., & Nunez, J. A. 1995, ApJ, 449, 231 1
Cooley, J. W., & Tukey, J. W. 1965, Math. Comput., 19, 297 1.3
Foreman-Mackey, D., Agol, E., Ambikasaran, S., & Angus, R. 2017, AJ, 154, 220 1
Gaia Collaboration, Prusti, T., de Bruijne, J. H. J., et al. 2016, A&A, 595, A1 1.3
Graham, M. J., Drake, A. J., Djorgovski, S. G., Mahabal, A. A., & Donalek, C. 2013a, MNRAS, 434, 2629 1
Graham, M. J., Drake, A. J., Djorgovski, S. G., et al. 2013b, MNRAS, 434, 3423 1, 1.3
Hernitschek, N., Schlafly, E. F., Sesar, B., et al. 2016, ApJ, 817, 73 1.3
Huijse, P., Estevez, P. A., Protopapas, P., Zegers, P., & Principe, J. C. 2012, IEEE Transactions on Signal Processing, 60, 5135 1
Jones, E., Oliphant, T., Peterson, P., et al. 2001–, SciPy: Open source scientific tools for Python, [Online; accessed 2017-01-19] 3
Kovács, G., Zucker, S., & Mazeh, T. 2002, A&A, 391, 369 2

Leroy, B. 2012, A&A, 545, A50 1.3
Lomb, N. R. 1976, Ap&SS, 39, 447 1, 4
LSST Science Collaboration, Abell, P. A., Allison, J., et al. 2009, ArXiv e-prints, arXiv:0912.0201 1.3
Palmer, D. M. 2009, ApJ, 695, 496 1.1, 2
Press, W. H., & Rybicki, G. B. 1989, ApJ, 338, 277 1, 1.3
Rasmussen, C. E., & Williams, C. K. I. 2005, Gaussian Processes for Machine Learning (Adaptive Computation and Machine Learning) (The MIT Press) 1
Scargle, J. D. 1982, ApJ, 263, 835 1, 4
Schwarzenberg-Czerny, A. 1996, ApJ, 460, L107 1.1
Sesar, B., Ivezić, Ž., Grammer, S. H., et al. 2010, ApJ, 708, 717 1.3, 4
Sesar, B., Hernitschek, N., Mitrović, S., et al. 2016, ArXiv e-prints, arXiv:1611.08596 1.3, 2.2.3, 2.2.3, 4
VanderPlas, J. 2016, gatspy: General tools for Astronomical Time Series in Python, Astrophysics Source Code Library, ascl:1610.007 4
VanderPlas, J. T., & Ivezić, Ž. 2015, ApJ, 812, 18 1.1, 1.1, 2.2.1
Vaníček, P. 1971, Ap&SS, 12, 10 1, 4
Zechmeister, M., & Kürster, M. 2009, A&A, 496, 577 1, 1.1